

Fluctuations of finite-time stability exponents in the standard map and the detection of small islands

Steven Tomsovic* and Arul Lakshminarayan†

Max-Planck-Institut für Physik komplexer Systeme, Nöthnitzer Strasse 38, D-01187 Dresden, Germany

(Received 11 June 2007; published 17 September 2007)

Some statistical properties of finite-time stability exponents in the standard map can be estimated analytically. The mean exponent averaged over the entire phase space behaves quite differently from all the other cumulants. Whereas the mean carries information about the strength of the interaction and only indirect information about dynamical correlations, the higher cumulants carry information about dynamical correlations and essentially no information about the interaction strength. In particular, the variance and higher cumulants of the exponent are very sensitive to dynamical correlations and easily detect the presence of very small islands of regular motion via their anomalous time scalings. The average of the stability matrix' inverse trace is even more sensitive to the presence of small islands and has a seemingly fractal behavior in the standard map parameter. The usual accelerator modes and the small islands created through double saddle node bifurcations, which come halfway between the positions in interaction strength of the usual accelerator modes, are clearly visible in the variance, whose time scaling is capable of detecting the presence of islands as small as 0.01% of the phase space. We study these quantities with a local approximation to the trace of the stability matrix which significantly simplifies the numerical calculations as well as allows for generalization of these methods to higher dimensions. We also discuss the nature of this local approximation in some detail.

DOI: [10.1103/PhysRevE.76.036207](https://doi.org/10.1103/PhysRevE.76.036207)

PACS number(s): 05.45.Ac, 45.10.-b, 45.05.+x

I. INTRODUCTION

A central and widely used measure of instability in dynamical systems is the Lyapunov exponent [1,2]. If a positive Lyapunov exponent is found for a continuous family of trajectories, then it is taken as a measure of their dynamical chaos. It is natural that the Lyapunov exponent, which is defined as a time-approaching-infinity limiting value, when calculated numerically, would be approximated by considering finite-time segments of the infinite history of a trajectory. This has led to the study of the so-called finite-time or local Lyapunov exponents (FTLEs) [2] in a variety of contexts. For example, FTLEs in one-dimensional maps [3–6], Hamiltonian systems [7–9], and advection and turbulent flows [10–12] form just a part of a rather large literature. Additionally in most experimental situations one encounters finite-time quantities. Such FTLEs have been the subject of numerous studies and have been experimentally measured in many contexts such as, for instance, in the study of passively advected particles [12]. There is also a very intimate relationship between the theory, methods, and measures found in the subject of Anderson localization [13] and FTLEs, although typically dynamical correlations are assumed vanishing or, if correlations are accounted for [14], then they are not the kind which is found in Hamiltonian flows where all the complexity of boundaries between chaotic and regular motion may exist. In other words these correlations are then calculated assuming that a typical trajectory covers phase space uniformly, whereas the presence of islands, however small, ensures that this is not true.

A very closely related, but less directly studied, quantity is the stability exponent which is defined via the eigenvalues of the stability matrix. A detailed study of this measure in relation to the Lyapunov exponent was carried out in [15] where it was conjectured that the Lyapunov and stability exponents were equal under a broad range of dynamical assumptions. It turns out that some of the studies that purported to be about the FTLEs have actually been studies of the stability exponents instead. In semiclassical mechanics, such as in the Gutzwiller trace formula [16], one of the natural classical quantities that appears is, in fact, the stability exponent and not the Lyapunov exponent. In higher-dimensional systems (larger than two degrees of freedom), it is the sum of the positive stability exponents that appears and in the infinite-time limit this tends to Kolmogorov-Sinai (KS) entropy. Since it has long been appreciated that the small-wavelength limit and the large-time limit in quantum mechanics are not interchangeable, we may expect that for fixed wavelength, it is the finite-time stability exponents, to be defined below more precisely, which may be relevant; see, for example, [17]. In fact, many of the interesting ways in which the fluctuations in the stability exponents might potentially show up in quantum mechanics and semiclassical theories remains to be investigated. This forms our primary motivation for studying the stability exponents, their distribution, and their scaling properties. Nevertheless, in this paper we restrict our attention to purely classical and low-dimensional systems [two-dimensional (2D) area-preserving maps] to establish basic properties and approximations, as well as to demonstrate their usefulness in detecting small stable dynamical structures. Naturally there are many parallels in the large literature on FTLEs both of a quantitative and qualitative character given that for a broad class of dynamical systems the infinite-time stability exponents are identical to the Lyapunov exponent. Our results

*Permanent address: Department of Physics and Astronomy, Washington State University, Pullman, WA 99164-2814, USA.

†Permanent address: Department of Physics, Indian Institute of Technology Madras, Chennai, 600036, India.

presented here generally for stability exponents are thus of relevance to the literature on FTLEs as well.

In the following section we first introduce the model in use throughout (the standard map) and an approximation for the stability exponent which provides a practical, calculational simplification that can be generalized to higher dimensions. Its ergodic value has corrections to the well-known formula of Chirikov [18]. In Sec. III, the local properties of the stability exponents are studied. We image the finite-time stability exponents in phase space and show their close relationship to the stable and unstable manifolds of the map and their connection to locating small nonhyperbolic regions. In Sec. IV, the fluctuations of the stability exponents are investigated and a formula for the ergodic average of the variance is derived. The scaling of the variance is shown to be a sensitive sensor for small islands. It is also shown that quantities that incorporate higher cumulants and that are of natural semiclassical relevance are even better sensors of such phase-space structures. In the Appendixes, formulas are collected for an expansion of the exact trace of the stability matrix as well as results for the time scaling of the stability exponent higher cumulants.

II. BACKGROUND, AN APPROXIMATION, AND ERGODIC AVERAGE

In this section we introduce the kicked rotor, provide definitions of the quantities of interest, explore an approximation of great practical utility, and use it to generate an improved analytic estimate of the Lyapunov exponent for the standard map.

A. Hamiltonian

Consider the 2D standard map [1,2] as a well-suited vehicle for our investigations. The methods and conclusions we reach will have wider applicability as this map represents the generic, local dynamics of any integrable system with shear in action-angle coordinates and shows how that structure gets altered by perturbation. A general kicked rotor is a mechanical-type particle constrained to move on a ring that is kicked instantaneously every multiple of a unit time $t = n\tau$. Supposing the radius of the ring to be $1/2\pi$ and $\tau=1$, the Hamiltonian takes the form

$$H(q,p) = \frac{p^2}{2} + V(q) \sum_{n=-\infty}^{\infty} \delta(t-n), \quad (1)$$

where $V(q)$ is a function periodic on the interval $q \in [0,1)$. From $H(q,p)$, mapping equations can be given:

$$\begin{aligned} p_{i+1} &= p_i - V'(q_i) \pmod{1}, \\ q_{i+1} &= q_i + p_{i+1} \pmod{1}, \end{aligned} \quad (2)$$

where we have made the choice to apply the potential kick before the free motion. The notation V' indicates the derivative of V with respect to q . We have also restricted the phase space to the unit torus ($q,p \in [0,1)$) for convenience; this is of no consequence for the results presented in this paper. The

simplest periodic function on a ring is just the lowest harmonic and leads to the standard map.

$$V(q) = -\frac{K}{4\pi^2} \cos(2\pi q). \quad (3)$$

Many results have long been known for the standard map [18]. At $K=0$ the map is integrable and is essentially a stroboscopic map of a freely rotating particle. There are both rational and irrational tori, depending on whether the frequency of rotation is commensurate or not with the frequency of the strobe. As the kicking strength is increased from zero with exactly the same frequency of stroboscopic observation, the incommensurate tori (irrational) survive small perturbations in accordance with the Kolmogorov-Arnold-Moser (KAM) theorem, while the commensurate (rational) ones break up into a pair of stable and unstable orbits in accordance with the Poincaré-Birkhoff theorem. The phase space becomes mixed with stable and chaotic orbits for increasing K . At around $K \approx 1$ the last rotational irrational KAM torus breaks and this leads to global diffusion. Up to $K=4$ a stable fixed point persists. Beyond $K \approx 5$ the standard map is considered to be largely chaotic, although it is also not proven to be completely chaotic for any value of K as far as we know. At an infinity of values of K stable fixed points are known to appear in the $p=0$ line for the map on the torus that are accelerator modes for the map on the cylinder [1]. These typically occupy regions in the phase space whose areas scale as $1/K^2$ [18]. Otherwise, the Lyapunov exponent of the map, to a very good approximation (Chirikov's result), increases with K as $\ln(K/2)$.

B. Finite-time stability exponents

For the map of Eq. (2), the stability matrix at time t is given by

$$M_t(q_0, p_0) = \prod_{i=0}^{t-1} M(q_i) = \prod_{i=0}^{t-1} \begin{pmatrix} 1 & -V''(q_i) \\ 1 & 1 - V''(q_i) \end{pmatrix}, \quad (4)$$

where the $M(q_i)$ are local one-step stability matrices. The finite-time Lyapunov exponents are defined via the singular values of M_t , which are the eigenvalues of $M_t^T M_t$ and turn out to be non-negative real numbers. The eigenvalues of stability matrices M_t , on the other hand, can in general be complex. To be technically correct we refer to the positive finite-time "stability exponents" (FTSEs) $\lambda_t(q_0, p_0)$, where the time t is the integer number of applications of the mapping equations and (q_0, p_0) is the initial condition. Consider only initial conditions (q_0, p_0) for which the orbits are unstable, in which case for 2D area-preserving maps such as we are presently studying the eigenvalues have to be real. The $\lambda_t(q_0, p_0)$ can be expressed in terms of the trace of the stability matrix as follows:

$$\begin{aligned}\lambda_t(q_0, p_0) &= \frac{1}{t} \ln \left| \frac{\text{Tr}[M_t(q_0, p_0)] + \sqrt{\text{Tr}[M_t(q_0, p_0)]^2 - 4}}{2} \right| \\ &\approx \frac{1}{t} \ln |\text{Tr}[M_t(q_0, p_0)]|,\end{aligned}\quad (5)$$

where $\text{Tr}(\cdots)$ denotes the trace operation. The approximation applies for t large enough. In that case, the approximation error is exponentially small in time except for stable trajectories. The generalization to higher dimensions is through the exponential growth rate of the magnitudes of the eigenvalues of the stability matrix (the Jacobian) at time t .

The natural quantity, which occurs in semiclassical expressions, is $|\text{Det}(M_t - I)|$ whose large-time behavior is determined by the sum of the positive stability exponents. For 2D area-preserving maps one has $|\text{Det}(I - M_t)| = |\text{Tr}(M_t) - 2|$ and the maximum stability exponent coincides with the KS entropy in the $t \rightarrow \infty$ limit. Thus, for the kicked rotor, studying $|\text{Det}(I - M_t)|$, $|\text{Tr}(M_t)|$, or the KS entropy is equivalent and our interest is in these quantities' (or their logarithms) finite-time fluctuations over phase space. Therefore our study is naturally close to the well-explored field of FTLEs. There are strong reasons to believe that in the infinite-time limit the definitions of FTLEs and FTSEs are equivalent in the chaotic cases that we are concerned with, although nongeneric examples are known for which this is not true [15]. Since we are dealing with finite-time measures we wish to be technically correct and refer to FTSEs, although these typically deviate from FTLEs by terms of the order of $1/t$. Recall that FTLEs can also be defined via the way initial error vectors y_0 grow in length:

$$\mu_t(q_0, p_0; y_0) = \frac{1}{t} \ln \left(\frac{\|M_t(q_0, p_0)y_0\|}{\|y_0\|} \right). \quad (6)$$

This definition of FTLEs has the added complication that they will depend on the initial error vector y_0 as well. However, in the infinite-time limit this corresponds to the exponent coming from the singular values of the limit of $M_{t \rightarrow \infty}$. Thus, μ_∞ is the Lyapunov exponent and it turns out not to have an initial condition dependence or fluctuations. There are reliable methods of evaluating each of these quantities [1, 19] (whether FTLEs or FTSEs) and they give essentially the same information, especially regarding the fluctuations of the exponents that we are primarily concerned with here. Higher-dimensional generalizations, which are currently under study [20], involve the fluctuations of $|\text{Det}(M - I)|$ and therefore we prefer to concentrate on FTSEs in this paper on 2D maps.

C. Approximating the trace

Before turning to a more detailed analysis of $\lambda_t(q_0, p_0)$, its average, variance, and higher-order moments and cumulants, we investigate approximations to the trace. These approximations make the trace calculations both efficient and simple, and extend to higher-dimensional systems, where they provide significant advantages. For any stability matrix of the form of Eq. (4), it turns out that $\text{Tr}[M_t(q_0, p_0)]$ can be expressed in an exact, closed form of products of the indi-

vidual traces $\text{Tr}[M(q_i)] = 2 - V''(q_i)$; the full expressions to all orders are found in Appendix A. We display here the zeroth-order approximation, indicated by $j=0$, and its first-order correction, indicated by $j=0+1$:

$$\text{Tr}[M_t(q_0, p_0)]_{j=0} = \prod_{i=0}^{t-1} [2 - V''(q_i)], \quad (7)$$

$$\begin{aligned}\text{Tr}[M_t(q_0, p_0)]_{j=0+1} \\ = \prod_{i=0}^{t-1} [2 - V''(q_i)] \left(1 - \sum_i^{\text{cyclic}} \frac{1}{[2 - V''(q_i)][2 - V''(q_{i+1})]} \right).\end{aligned}\quad (8)$$

These expressions represent well the large- K behavior of the exact trace $\text{Tr}[M_t(q_0, p_0)]$, even though, *a priori*, one might suspect that estimating this trace by Eq. (7) is rather inadequate. After all, consider the fact that the leading correction, shown in Eq. (8), contains t terms of inverse products of pseudorandom factors which have the possibility of nearly vanishing. Crudely speaking, as multiple trajectories are considered or as t increases for an individual trajectory, it becomes more and more likely that a nearly vanishing factor will be encountered, thus creating a correction term that dominates the leading term. Worse, all the successive corrections involve combinations of the same products of inverse factors (Appendix A). It is possible that no particular correction term dominates either.

Fortunately and oddly enough, Eq. (7) (the $j=0$ term) is an excellent approximation and, in fact, is more than adequate for analytically estimating the leading asymptotic behaviors of the finite-time stability exponents. It is even good enough to capture the power laws for both local averages and variances of FTSEs, which we investigate ahead.

Figure 1 compares for a single trajectory the natural logarithm of the exact trace, the product form estimation of Eq. (7), and the estimation of Eq. (8) where the mean exponential increase has been subtracted from all three in the first panel. In these panels several general features are readily seen. As a function of time, the leading approximation follows the exact trace time step by time step except for sudden vertical displacements at time steps where the factor $|2 - K \cos(2\pi q)|$ nearly vanishes. In this example, the corrected approximation follows the exact trace longer in time before departing, although this does not have to be the case. A second point is that the exponential growth dwarfs the errors of the approximation. Even though the approximation of Eq. (7) is off by a factor of roughly $\sim e^{4 \leftarrow 6}$ before $t=300$, this is miniscule compared with the average exponential growth of the trace (in this example it is $\exp[t \ln K/2] = 4^t$) and so it alters the stability exponent very little. From the form of the leading correction, a Lévy-flight nature might be expected for the corrections. This can be seen in the natural logarithm of the ratio of Eqs. (7) and (8), respectively, where only a couple of jumps dominate the differences between the zeroth and first approximations. Although not shown, as K increases, a corresponding curve seems to be rather "quiet," punctuated by relatively fewer jumps.

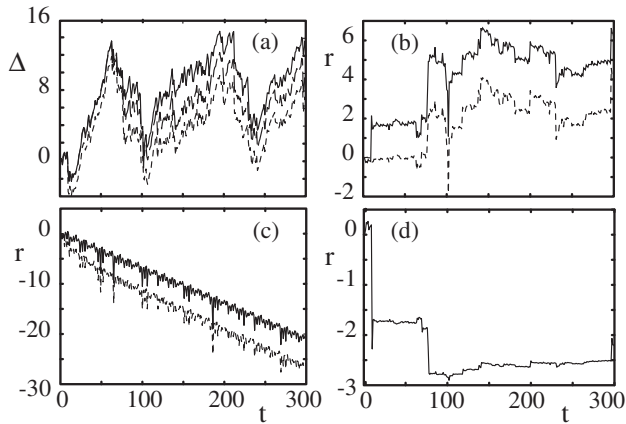


FIG. 1. Comparison of the two approximations, Eqs. (7) and (8), for the trace of $M_t(q_0, p_0)$ with the exact value. In panel (a), the three curves are for $K=8$ with the initial condition $(q_0, p_0) = (0.3, 0.6)$, $\Delta = \ln |M_t(q_0, p_0)| - t \ln(K/2)$, the exact trace is the solid line, the $j=0$ approximation is the dotted line (lowest), and the $j=0+1$ approximation is the dashed line. In panel (b), $r = \ln[|M_t(q_0, p_0)| / |\tilde{M}_t(q_0, p_0)|]$. For the solid line, $\tilde{M}_t(q_0, p_0)$ is evaluated to the $j=0$ approximation, and for the dashed line, $\tilde{M}_t(q_0, p_0)$ is evaluated to the $j=0+1$ approximation. Similarly to panel (b), in panel (d), the ratio of the two approximations is given. Panel (c) is similar to panel (b), except that $K=9.28$ with the initial condition $(q_0, p_0) = (0.19, 0.38)$ (which is a stable trajectory). The solid line is for the $j=0$ approximation whereas the lower curve is for the $j=0+1$ approximation.

These approximations naturally are worst for segments of trajectories that are stable or nearly stable. For them, $2 - V''$ is repeatedly close to zero. The large value of K thus does not order corrections. An example is given of a nearly stable trajectory in a region near a double saddle point bifurcation. The value of K is larger than used previously to illustrate the behavior of a highly unstable orbit. Nevertheless, the approximation is far worse. On the other hand, however, it gives a stability (or Lyapunov) exponent of about 0.067, a small number compared with $\mu_\infty \approx 1.53$. As long as the percentage of stable and nearly stable orbits is very small, the errors in using Eq. (7) for all the orbits regardless of their nature are small after averaging over initial conditions. For the usual Lyapunov exponent there exists a “local” expression which is in some sense the equivalent of the $j=0$ expression for the trace we have just examined [3].

Finally, note that the approximation scheme introduced here extends to a far larger class of dynamical systems than the kicked rotors under study. There are at least three generalizations possible in a strict sense. First of all, the determinant at each time step does not have to be unity; it only has to be constant. Thus, this approximation is perfectly well adapted and applicable to maps with constant dissipation, such as the Hénon map. The regime of validity is determined by the dominance of the leading product term, and either strong dissipation [33] or strong chaos (or some combination) is sufficient to ensure this condition. Second, it is possible to discretize continuous Hamiltonian dynamical systems and make a limiting process to calculate the stability

matrix. Thus, one anticipates that a limiting process for short time steps leads to a differential form of this approximation applicable to unstable trajectories for continuous Hamiltonian systems of the type having a mechanical momentum plus some position-dependent potential (or any Hamiltonian which can be rendered into this form by canonical transformation). Third, as alluded to previously, it is possible to generate a similar approximation for multiple-degree-of-freedom systems. However, the approximation is naturally extended to $\text{Det}(M-I)$ and is much more cumbersome for $\text{Tr}(M_t)$ [20]. Last, we mention that even if the conditions for applicability are not strictly met, it seems likely that a related approximate scheme still holds due to the rapid alignment of the stretching directions in phase space.

D. Average finite-time stability exponents

Much of what is known applies readily if a product form can be found for $\text{Tr}[M_t(q_0, p_0)]$. This is precisely what the kicked rotor has for sufficiently strong potentials and times not too long. There the $j=0$ term would be sufficient, and from Eqs. (5) and (7), the $\{\lambda_t(q_0, p_0)\}$ are approximately given by

$$\lambda_t^0(q_0, p_0) = \frac{1}{t} \sum_{i=0}^{t-1} \ln|2 - V''(q_i)|. \quad (9)$$

The superscript 0 indicates that it is the zeroth-order approximation. Assuming that the system is fully chaotic, the expectation value is given by integrating (averaging) over all initial conditions and

$$\begin{aligned} \langle \lambda_t^0 \rangle &= \int_0^1 dq \int_0^1 dp \lambda_t^0(q, p) = \frac{1}{t} \sum_{i=0}^{t-1} \int_0^1 dq \ln|2 - V''(q)| \\ &= \int_0^1 dq \ln|2 - V''(q)|. \end{aligned} \quad (10)$$

For the standard map, the result is $\langle \lambda^0 \rangle = \ln \frac{K}{2}$; the integral is evaluated *exactly*. Not surprisingly, this coincides exactly with the Lyapunov exponent approximation made by Chirikov [18] even though this result is for the stability exponent. The phase-space mean of the finite-time stability exponent is *independent* of integration time and time is dropped from its notation. This indicates that the mean is to within approximations made so far equal to μ_∞ . In contrast, the entire phase-space average of the FTLE is not equal to its infinite-time ergodic average, but has a transient that decays as a power law in time and in the absence of significant islands of regular motion goes as $1/t$.

We plot the mean stability exponent in Fig. 2. It is interesting that there is a simple systematic correction to the well-known formula of Chirikov above that is of the order of $1/K^2$ and that, other than the value of K (excluding sample size noise), there is essentially no indication of any other kind of dynamical information.

The origin of the corrections lie in the terms with $j \neq 0$ in the approximations to the exact trace; however, its rigorous derivation seems fraught with difficulties. A somewhat heu-

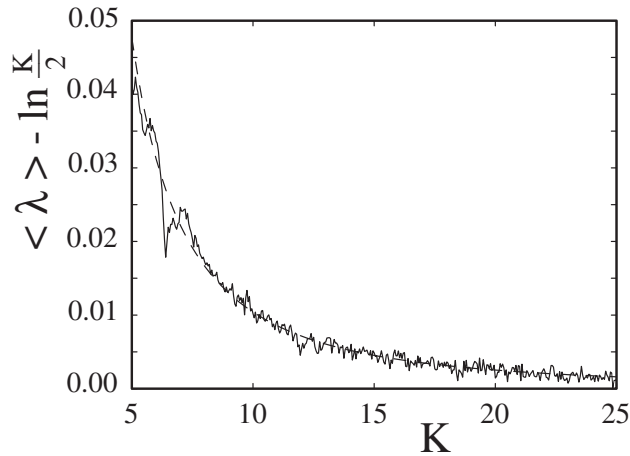


FIG. 2. The exact mean stability exponent calculated as a function of kicking strength with the zeroth-order approximation $\ln(K/2)$ subtracted. Other than small oscillations, the difference is seen to be almost exactly equal to the first correction $(K^2-4)^{-1}$, given in Eq. (16). This is plotted as the dashed curve.

ristic derivation of the $1/K^2$ correction to Chirikov's expression can be derived from Eq. (8). The product term gives an independent contribution and is exactly $\ln K/2$ as already noted. Subtracting that term, one is left with the ergodic average of at least the $j=1$ term to determine the correction:

$$\delta\lambda(K) = \frac{1}{t} \left\langle \ln \left| 1 - \sum_i^{\text{cyclic}} \frac{1}{(2 - K \cos 2\pi q_i)(2 - K \cos 2\pi q_{i+1})} \right| \right\rangle. \quad (11)$$

We are not aware of a way to evaluate this integral without making a few simplifications. Consider first that the correction is essentially being expanded about $K=\infty$ or in other words the expansion is about $\epsilon \equiv 1/K=0$. In this limit at some fixed value t , the probability is vanishing that more than one factor of $|2 - K \cos 2\pi q_i|$ for a given trajectory is close enough to zero that it can meaningfully contribute. Let q_0 denote the q value for the minimum of the set of $|2 - K \cos 2\pi q_i|$. Although that involves two terms in the series, only one will dominate. However, since there are t terms in the cyclic sum, there are t ways this can happen; together this is consistent with what happens in the subject of extreme statistics. The basic expression to be evaluated is

$$\delta\lambda(K) \approx \left\langle \ln \left| 1 - \frac{1}{(2 - K \cos 2\pi q_0)(2 - K \cos 2\pi q_1)} \right| \right\rangle. \quad (12)$$

Due to the momentum not entering the expression, $\{q_0, q_1\}$ can be integrated as two independent variables, each uniformly distributed on the interval $[0, 1)$. The next step follows from the discontinuity in the expression for the integral:

$$\int_0^1 dq \ln|a \pm b \cos 2\pi q| = \begin{cases} \ln \frac{|b|}{2}, & |b| \geq |a|, \\ \ln \frac{|a| + \sqrt{a^2 - b^2}}{2}, & |a| \geq |b|. \end{cases} \quad (13)$$

It is straightforward to verify that to the extent that the upper form of the integral applies, the expression for $\delta\lambda(K)$ vanishes. Therefore it turns out that only values of q_0 for which

$$-\frac{1}{K-2} \leq 2 - K \cos 2\pi q_0 \leq \frac{1}{K+2} \quad (14)$$

contribute a correction to the average stability exponent and the limits of integration on q_0 are restricted to that domain (actually there are two such domains). Switching variables to $y=2-K \cos 2\pi q_0$, one has (accounting for both domains)

$$\delta\lambda(K) = \frac{1}{\pi} \int_{-1/(K-2)}^{1/(K+2)} \frac{dy}{\sqrt{K^2 - (2-y)^2}} \times \left(\ln \left| \frac{1 - 2y + \sqrt{(1-2y)^2 - K^2 y^2}}{2} \right| - \ln \frac{K|y|}{2} \right). \quad (15)$$

If the leading square-root factor is expanded in a series of powers of y , the integrals can be analytically evaluated. This gives

$$\delta\lambda(K) = \frac{1}{K^2 - 4} + \frac{19}{6(K^2 - 4)^3} + \frac{4}{(K^2 - 4)^4} + \frac{24}{(K^2 - 4)^5} + \dots \quad (16)$$

As seen in Fig. 2, the first term accounts completely for the overall correction to the Chirikov result to the accuracy level of the numerical calculations. The $j=1$ trace correction appears to have given properly the stability (Lyapunov) exponent to $O(K^{-6})$. This is interesting because it seems that it is not necessary to consider the $j=2$ and higher corrections to the trace whereas one might have naively expected the $j=2$ trace correction to give an $O(K^{-4})$ contribution. Chirikov's accurate estimate for the Lyapunov exponent also has the same corrections derived above. This may be expected as at infinite times the Lyapunov and stability exponents indeed converge for the standard map. However, numerical calculations of the FTLE, even averaged over the entire phase space, mask this with transients that are of the order of $1/(tK)$.

III. LOCAL PROPERTIES OF FINITE-TIME STABILITY EXPONENTS

The FTSE $\lambda_i(q_0, p_0)$ is also a *local* stability exponent as emphasized by its dependence on initial conditions. The mean over a local "area" \mathcal{A} that is much smaller than the entire phase space (Ω) includes transients that are power laws in time. Its interesting variations over phase space can be displayed by assuming the following particular form:

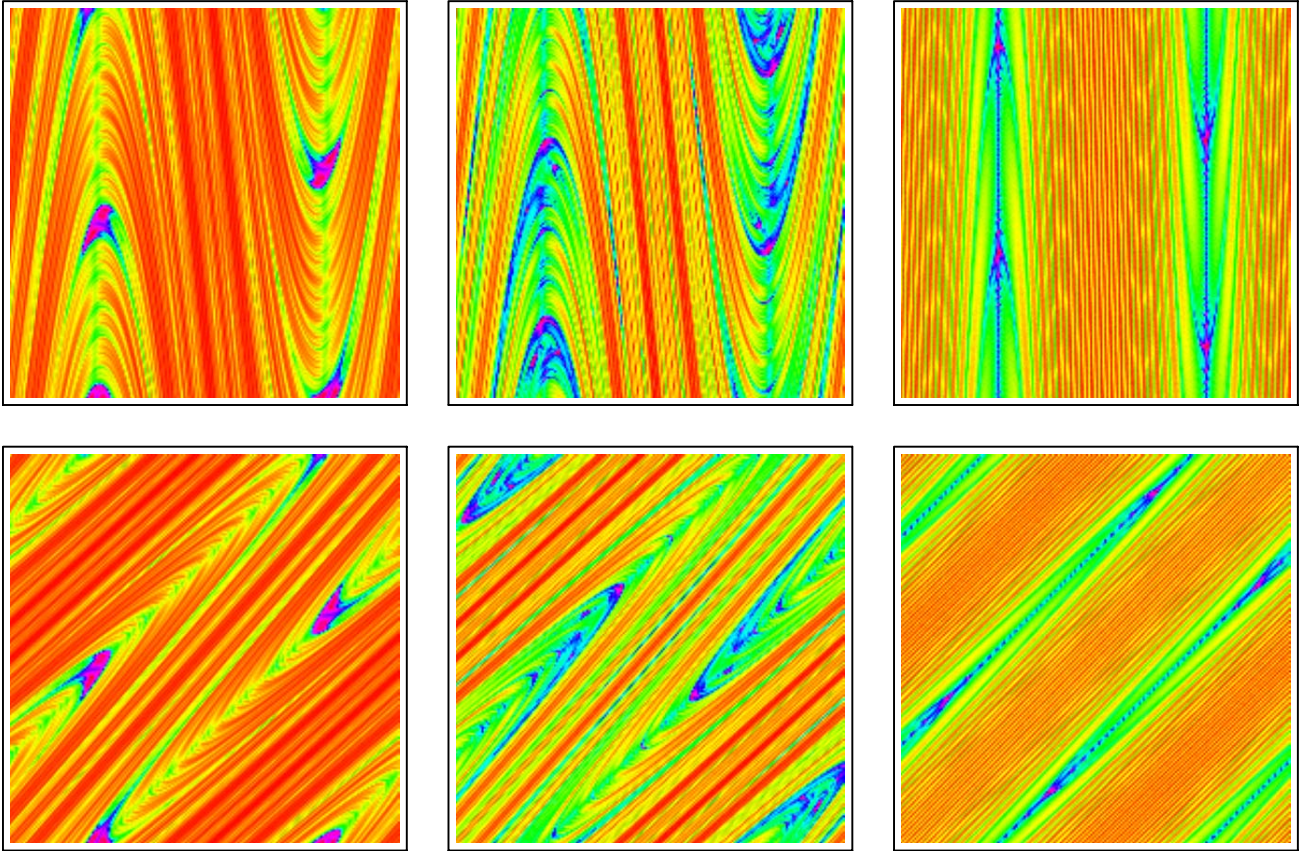


FIG. 3. (Color online) A density plot of the average $\langle \lambda_{\pm 10}(q_0, p_0) \rangle_{\mathcal{A}}$ (top, bottom respectively) as a function of (q_0, p_0) . High to low density is indicated as a color transition from purple to red (black to gray). The area \mathcal{A} over which the averages are calculated are squares of area 0.005^2 . The case $K=10$ (center column) has no apparent stable islands, whereas at $K=9.26$ (left column) there are two small islands each of period 4 where the density is enhanced and purple (black; see the next figure for a magnification of the dynamical structure underlying this zone). Note the prominent linear structures for a large value of $K(=40)$ in the right column.

$$\langle \lambda_{\pm 10}(q_0, p_0) \rangle_{\mathcal{A}} = \frac{C_{\mathcal{A}}}{t^{\gamma}} + \ln(K/2) + \frac{1}{K^2 - 4} + O(K^{-6}). \quad (17)$$

The area \mathcal{A} is ideally a very small local region of the available phase space centered at (q_0, p_0) , and the final two terms are responsible for removing μ_{∞} , thus leaving just the fluctuating part. Here $K \gg 5$ (in practice $K > 6$) and the time t is larger than the logarithmically short mixing time scale $\tau_m = \ln(\Omega/\mathcal{A})/\mu_{\infty} \approx \ln(1/\mathcal{A})/\ln(K/2)$. This time scale arises as the “log time” during which the initial region of volume \mathcal{A} through propagation essentially elongates to the extent that it enters each distinct local region of area \mathcal{A} once on average. The averaging in the left-hand side (LHS) of the above expression is over the uniform Lebesgue measure, which is the invariant measure of the map. Note that when the *entire* phase space—i.e., the unit square for the kicked rotor—is used for averaging the FTSE, the transients in time seem to be exponentially small and essentially $C_{\Omega}=0$.

Expressing the finite-time stability exponents in this way allows us also to draw attention to anomalous features that may be present for various values of K , especially those with small, but significant, stable islands in phase space that sur-

vive for large K , such as the accelerator modes. The quantity $C_{\mathcal{A}}$ fluctuates in both time and phase-space points around which the averaging is done; it can also have a strong dependence on K . The index γ serves to remove the principal nonfluctuating time scaling part of the FTSE and determines the rate at which it approaches the ergodic average. For example, in the case when there are no apparent small islands $\gamma=1$ (see text ahead), while in the presence of stable regions $0 < \gamma < 1$. The area \mathcal{A} serves as a region of coarse graining, and it must be emphasized that unless we choose \mathcal{A} to be the entire phase space (Ω), the regions will exclude regular islands and trajectories. We present results for an exponent similar to γ when studying the variance below. Previous studies of the FTLE have also presented such forms of convergence to the infinite-time Lyapunov exponents [15,21,22], but typically in dissipative systems.

To get an idea of the complexity of the phase-space distribution of FTSEs as we move (q_0, p_0) around, always averaging over a small area \mathcal{A} of phase space centered at this point, we display density plots in Fig. 3.

The figure shows forward and backward in time evolution for three cases of K : namely, 9.26, 10, and 40, respectively. The intricate structures that arise highlight areas of reduced

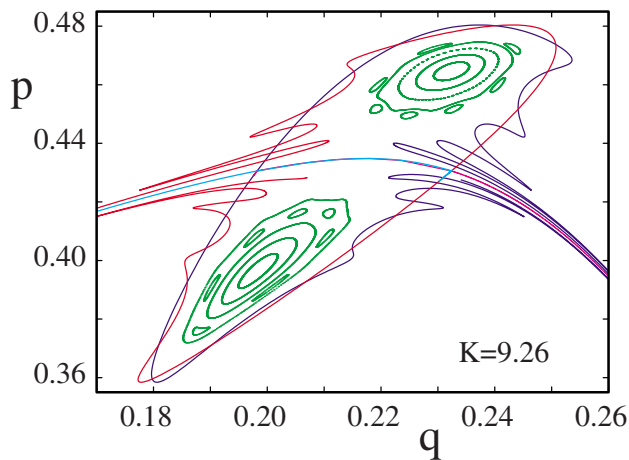


FIG. 4. (Color online) Expanded plot of two islands of period-4 regular motion and the stable and unstable manifolds associated with two unstable orbits born at the same double saddle node bifurcation ($K=9.20667769750$) as the islands themselves. Only one of this structure’s four images is plotted. Transport in and out of the inner region is severely limited by the small turnstile fluxes visible.

hyperbolicity and hence smaller FTSEs. For the case of forward evolution in time, trajectories which are trapped in more stable areas or propagate into those areas have lowest stability and appear purple (black). Those trajectories propagating into more stable zones must do so in a direction aligned along the greatest exponential compression. This direction is determined by the stable manifolds of the short periodic orbits. Thus, one sees a structure that mirrors the foliation of phase space by these stable manifolds in the top row of the figure. Similarly, for reverse evolution in time, one sees a structure that mirrors the corresponding unstable manifolds in the lower row. In the first column, the phase space has small islands, while the center column, $K=10$, does not have such prominent islands. The absence of a detectable island of regular motion results in a less contrasted variation of the FTSE. At $K=40$ (right column), which is very strongly chaotic, there are linear regions of low FTSEs that are clearly visible. However, any other regions have more or less merged into the background. These linear regions coincide with the K -independent borders of the nonhyperbolic regions for a one-step forward (the vertical lines at $q=1/4$ and $q=3/4$) and one-step backward iteration (the lines $q-p-1/4=0 \pmod{1}$ and $q-p-3/4=0 \pmod{1}$). The fact that these lines are not dense in the phase space and survive for long times at large K underlies the coexistence of strongly chaotic dynamics with the fact that the map may not possess a single K value for which it becomes mathematically fully hyperbolic. Similar plots of FTLEs were given earlier in the context of area-preserving maps for smaller values of K [23] and passive scalar advection [11].

It is possible to use this plot to help locate small islands. Investigating the purple (black) zones seen in the left column of Fig. 3 more closely reveals the interesting structure found in Fig. 4.

It arises for K values greater than approximately 9.2, at which point there is a double saddle node bifurcation. As K

increases from the bifurcation, the structure grows to a maximum size near $K=9.26$. The full structure includes not only the small stable islands, but also the short unstable periodic orbits along with their homoclinic tangles—i.e., crossings of stable and unstable manifolds. The turnstiles formed by these crossings limit the rate trajectories can move in and out of the region surrounding the islands of stable motion [24]. Therefore, in this structure, it is not just the immediate interface between the chaotic and regular motion which is generating trapping, although that, of course, is happening additionally just beyond the outermost tori pictured. In fact, chaotic trajectories may remain trapped inside the tangle for hundreds or more time steps in the roughly 2/3 portion outside the islands themselves. For this reason, the entire structure was visible in Fig. 3, not just the islands, and multiple trapping time scales would be expected. One of the more unusual features is a highly asymmetric instability (factor of 1000 or so) in two of the stable and unstable manifolds pictured. The interior middle line is actually a stable and unstable manifold whose turnstile is so tiny as to appear as a single line dividing the interior, thus making transport between the upper and lower regions nearly nonexistent.

IV. FLUCTUATIONS OF THE FINITE-TIME STABILITY EXPONENT

The statistical properties of $\{\lambda_t(q_0, p_0)\}$ can be studied via the construction of a probability density $\rho_{\lambda_t}(x; t)$ —i.e., the probability of finding λ_t in the interval dx centered at x . For a large class of chaotic systems, a great deal is known about general properties of $\rho_{\lambda_t}(x; t)$, although strictly speaking just for FTLEs. The approach to a unique Lyapunov exponent is connected to $\rho_{\lambda_t}(x; t)$ approaching a δ -function limit as $t \rightarrow \infty$. Through the study of the density’s cumulants for fully hyperbolic systems, one sees that there is a slow approach to an ever narrower, roughly Gaussian density as $t \rightarrow \infty$ [2]. A detailed study with analytic results has also been performed for “white-noise” random media [25]. Interestingly enough, it is also known that this limiting process is too slow to understand the behavior of the generating function for the cumulants $\nu_n(t)$,

$$\ln \langle \exp mt\lambda_t \rangle = \sum_{n=1}^{\infty} \nu_n(t) \frac{(mt)^n}{n!} \approx \ln \langle |\text{Tr}(M_t)|^m \rangle, \quad (18)$$

which is also a quantity of direct interest in semiclassical studies or the theory of Anderson localization. This relation should be thought of as an expansion in the real variable m .

If one were to calculate the full probability density $\rho_{\lambda_t}(x; t)$ for the kicked rotor, one would see that it qualitatively takes on one of two forms. If the kicking strength is set to a value at which there is no discernible evidence for any stable orbits (no detectable nonexponentially decaying dynamical correlations), the density has a well-defined peak near the Lyapunov exponent and is not too far off a Gaussian form. If the kicking strength is set to a value at which both stable and strongly chaotic trajectories coexist in the phase space, then it takes on a bimodal form with a peak near the mean Lyapunov or stability exponent and another represent-

ing algebraic behavior near zero [7]. The density is continuous between the two peaks. Nevertheless, as $t \rightarrow \infty$, a unique Lyapunov exponent emerges, albeit much more slowly. This has a profound effect on the time-scaling properties of the density or, more specifically, its cumulants (moments) with the exception of its mean. The algebraic peak and the “neck” connecting the two peaks disappear in the $t \rightarrow \infty$ limit very differently than the rate at which the width of the main peak narrows. Time scaling therefore gives a great deal of information about nonhyperbolicities.

The work of Sepúlveda *et al.* [7], extending the foundation from Grassberger *et al.* [21], showed that the power spectra of unstable orbits had two features of sharp and broad peaks, which could be separated out and associated, respectively, with portions of the trajectory nearby stable and unstable dynamical regions, effectively locating regions of regular dynamics. Below, we focus on a simpler time-scaling property of moments that also is capable of locating regions of regular dynamics. Generally speaking, their method and ours become more and more difficult to apply as the size of the regular regions decreases. However, we show ahead that time scaling is nevertheless very sensitive and capable of locating rather small regions. We are uncertain whether the power spectrum method is as sensitive.

A. Time scaling of the variance

We proceed next to a more detailed analysis of the variance (second cumulant) by first deriving the contributions that neglect dynamical correlations, which leads to an explicit formula for the standard map; the first cumulant (the mean) is already treated above. It is shown that while the general time scaling of the variance is $1/t$, this is significantly modified by the presence of even very small stable islands, thus providing a practical way of detecting a “barely” mixed phase space. We anticipate that this would be especially useful in its higher-dimensional generalizations [20]. A first study appears to support our expectations [26].

The variance of the FTSE over Ω can be expressed simply using the approximation of Eq. (7) for the exact trace; the exact one $\nu_2(t)$ differs from its approximation above, $\nu_2^0(t)$, by very small amounts which can be ignored. One finds

$$\nu_2^0(t) = \int_0^1 \int_0^1 dq_0 dp_0 \left(\frac{1}{t} \sum_{i=0}^{t-1} \ln|2 - V''(q_i)| \right)^2 - (\nu_1^0)^2. \quad (19)$$

The variance may be separated into a term that is explicitly independent of dynamical correlations and a series of terms that contain the contributions of dynamical correlations, which, respectively, are

$$\begin{aligned} \nu_2^0(t) &= \frac{1}{t} \int_0^1 \int_0^1 dp dq [\ln^2|2 - V''(q)| - (\nu_1^0)^2] \\ &+ \frac{2}{t^2} \sum_{\tau=1}^{t-1} (t - \tau) \int_0^1 \int_0^1 dp_0 dq_0 \\ &\times [\ln|2 - V''(q_0)| \ln|2 - V''(q_\tau)| - (\nu_1^0)^2]. \quad (20) \end{aligned}$$

The contribution of the first term above is

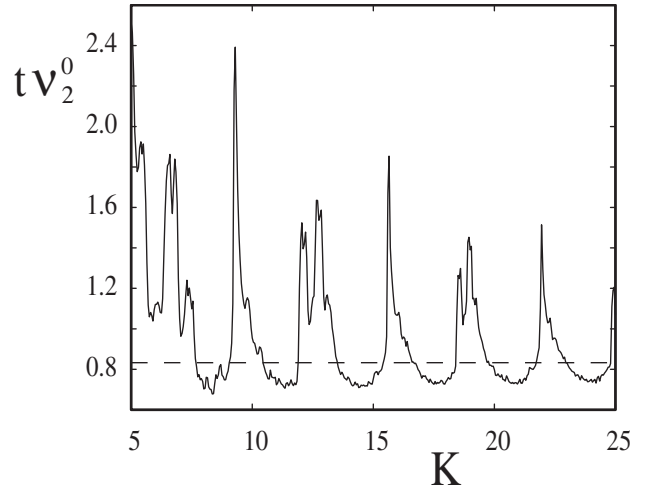


FIG. 5. The $j=0$ order calculation of the variance as a function of kicking strength. It is multiplied by t and averaged over $t=150$. It illustrates that the variance is very sensitive to dynamical correlations. The dashed line at $\pi^2/12$ is the value of the integral from Eq. (21).

$$\begin{aligned} \frac{1}{t} \mathcal{X}_2 &\approx \frac{1}{t} \int_0^1 dq [\ln|K \cos(2\pi q)| - \ln(K/2)]^2 \\ &= \frac{\pi^2}{12t} = \frac{1}{t} 0.822 \dots \quad (21) \end{aligned}$$

Here we have introduced \mathcal{X}_2 as a term that does not carry correlation information.

Depending on the system, strong behavior connected to dynamical correlations, but not reflected in the mean, is possible in the variance, which the summation above makes clear. Note that the dynamical correlation function is bounded for a broad class of potentials. Furthermore, as long as the correlations decay faster than τ^{-1} , they cannot alter the basic time dependence of the variance. If they decay more slowly, they could well become the leading contribution in time. As seen in Fig. 5 the variance is strongly dependent on the value of the kicking strength K and shows marked peaks at various values.

These include conventional accelerator modes as well as other stable islands, such as those illustrated in Fig. 4 that appear near $K=9.3$.

B. Variance as a sensor for small elliptic islands

As just noted, the variance scales with time differently from the $1/t$ law above as a result of correlations decaying as slow or more slowly than τ^{-1} . For the kicked rotor, consider ensembles of trajectories that originate from small regions \mathcal{A} of the phase space rather than the whole space; the reduced averaging region is motivated by the interest in a process that more practically generalizes to systems with greater numbers of degrees of freedom. The average behavior $\langle \lambda_t^0(q_0, p_0) \rangle_{\mathcal{A}}$ may obscure the scaling by the presence of the infinite-time asymptotic value, whereas the fluctuations die out asymptotically and are more stable for evaluating power laws, al-

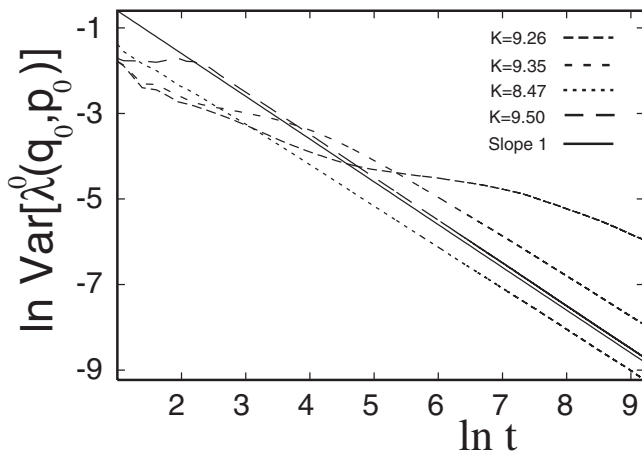


FIG. 6. The scaling of the variance for an ensemble of 40000 initial conditions uniformly distributed in the square $\mathcal{A} = \{(0.10, 0.10), (0.15, 0.15)\}$.

though note that “wiggles” in the FTLE were attributed to stability islands in an earlier work on kicked tops [27]. The variance can be written

$$\text{Var}[\lambda_t^0(q_0, p_0)]_{\mathcal{A}} = D_{\mathcal{A}} t^{\alpha}, \quad (22)$$

where $\nu_2^0(t) = \text{Var}[\lambda_t^0(q_0, p_0)]_{\Omega}$. After accounting properly for the $t^{-\alpha}$ dependence, one sees that $D_{\mathcal{A}}$ fluctuates as a function of time similarly to a diffusive variable. Generally speaking, the greater the time range over which α is calculated and the greater the number of trajectories run, the greater precision with which α is determined. In this regard, the simplicity of the $j=0$ approximation is quite helpful because it makes it possible to increase both in a practical sense. One suspects that the smaller and less influential the island of regular motion, the closer α approaches unity and thus α accuracy is directly linked to how small an island one can detect in this way. Earlier works such as [28,29] have studied scaling laws that arise in the fluctuations of the FTLE and have already emphasized the role of sticky regions and islands. Ahead, we show islands of measure roughly 0.01% of Ω that were found with the FTSE time scalings relatively easily.

In Fig. 6 we show the scaling of the FTSE variance for a few values of the kicking parameter compared with $\alpha=1$.

The regular island structures of Fig. 4 at $K=9.26$ have a very significant effect on the time scaling. One also sees the appearance of more than one time scale—i.e., slope—depending on the time regime. The turnstiles previously pictured would at first lead to only small numbers of trajectories entering into the interior region of the homoclinic tangle, and one would expect α to begin close to unity. Later, a certain proportion would get trapped inside for up to hundreds or thousands of time steps. During this period, the greatest proportion would resemble nearly stable orbits and α would deviate most from unity. Further in time, only the trapping right at the regular island-chaos interface would contribute to deviations from unity and the slope increases somewhat again. It is known that different trapping mechanisms can coexist in phase space and lead to a “multifractal” process [30]. This particular example is instructive because the turn-

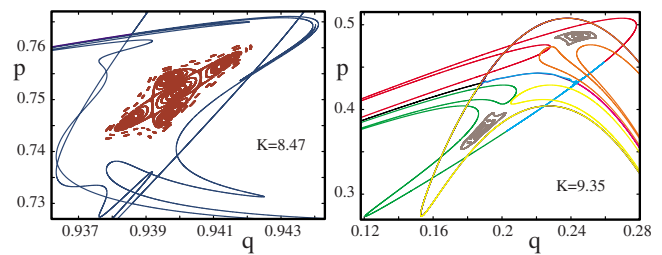


FIG. 7. (Color online) Small regular islands found at $K = (8.47, 9.35)$ and their surrounding homoclinic tangles. Not only are the islands much smaller than for $K=9.26$, but the turnstile fluxes are larger relative to the measure of the enclosed area, making the flow much less restricted in the neighborhoods of the islands. The measure of the regular region for $K=8.47$ is roughly 0.01% of Ω , counting all the unique iterations of the structure.

stile time scale is fairly well separated from the others. The smaller the stable islands, the more the power laws recover the uncorrelated $1/t$ form. At $K=(8.47, 9.35)$ there are only small detectable deviations from unity, and in both cases it is possible to locate very small islands; see Fig. 7.

At $K=9.5$ we could not locate islands in this way and the exponent α is as close to unity as the precision of the calculation.

It is worthwhile remarking that while accelerator modes give rise to anomalous diffusion (in momentum) in the standard map on the cylinder [31], the different scaling regimes discussed above hold whether the stable regions are accelerator modes or not. However, the suppression of the variance’s approach to zero and the average Lyapunov or stability exponent to the ergodic average in the presence of small islands have similar origins. Namely, they are due to trajectories spending intermittently long intervals of time near sticky islands or regions of almost marginal stability and nonhyperbolicity.

We point out that although power laws such as that given in Eq. (22) are susceptible to variations in the initial position (q_0, p_0) , to changes of the trajectory sampling, and to the time window in which they are under study, the α deviations from unity are robust structures and can be correlated to phase-space structures.

In Fig. 8 we show the variation of α as K is tuned through a range which has small stable regions. The “normal” exponent $\alpha=1$ is realized to a very good approximation for most values of K , indicating the general absence of significantly large, low-instability traps. The prominent deviation around $K=9.3$ is due to the structure of Fig. 4 born out of a double saddle node bifurcation around $K=9.2$ and it persists to near $K=9.45$. It grows to its largest size around $K=9.26$ where the variance decays the most slowly, $\alpha \approx 0.16$. In terms of the phase-space area, the islands occupy approximately 0.5% of Ω at $K=9.26$ and 0.2% at $K=9.35$ (for which $\alpha \approx 0.88$). Notice robust, though small, deviations from unity at several other values of K . For example, even for an island as small as that found at $K=8.47$ (0.01%, $\alpha \approx 0.96$), there is a range of K values where α is significantly and consistently different from unity; the inset shows a finer scan of this region. The fine oscillatory structure that is apparent here could be

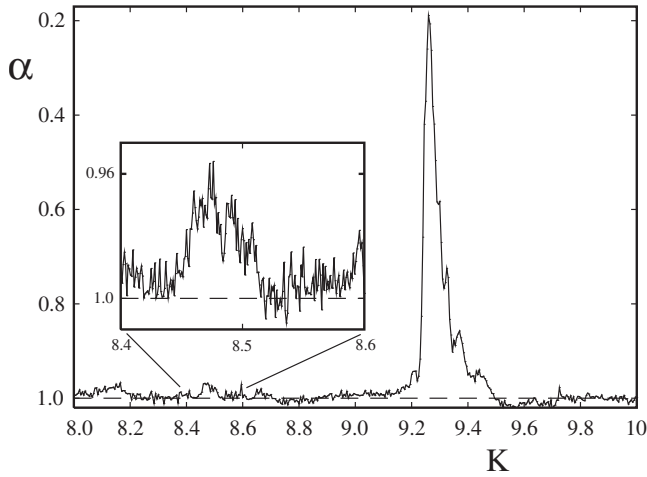


FIG. 8. The exponent α in the decay of the variance of the FTSE as a function of the kicking strength K . The ensemble is the same as that used in Fig. 6. A region around $K=8.47$ is shown at a resolution of 0.001 in K .

reflecting the fractal behavior of such exponents themselves which in turn are due to bifurcations in the map that produce or destroy very tiny islands almost continuously. The Newhouse phenomenon wherein homoclinic tangencies produce an infinite number of sinks is replaced in conservative scenarios by a large number of elliptic islands [32]. Knowing that there is possibly an island somewhere in phase space does not locate it, and a blind search could well be futile. Some direction is important. The islands are found more easily by searching around regions of the lowest stability exponent, regions that are highlighted in figures such as Fig. 3 and correspond to zones of low hyperbolicity. Note one last observation, that for the three islands constructed, $K=(9.26, 9.35, 8.47)$, the degree of α 's deviation from unity and the measure of the islands are in corresponding order, smallest to largest.

C. Higher-order cumulants

Similar more complicated dynamical correlation expressions enter for all the higher cumulants. They naturally give more weight to the extremes of the probability density, and thus, one might expect them to be even more sensitive to stable islands. To be useful, they also need a standard time scaling for their correlation-independent components as found for the variance. In fact they do have a simple time dependence and it involves generalizations of \mathcal{X}_2 . By defining

$$\mathcal{X}_n = \int_0^1 \int_0^1 dp dq [\ln|2 - V''(q)| - \nu_1^0]^n, \quad (23)$$

the correlation-independent components of the higher-order cumulants are expressible as polynomials in these quantities with a single overall power-law decay in time and no other parametric dependences. Details are presented in Appendix B, but note here an interesting consequence of these expres-

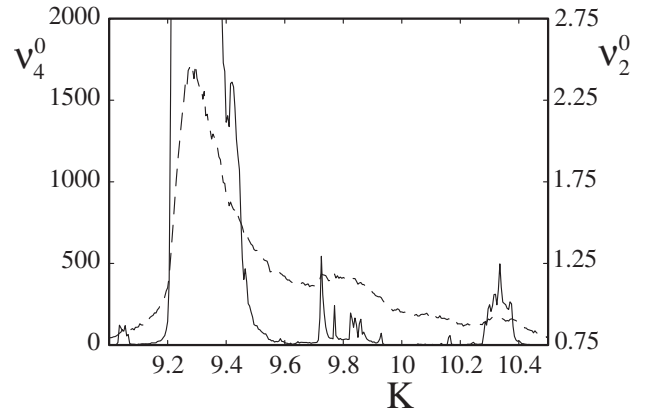


FIG. 9. The fourth and second cumulants as a function of K using the $j=0$ approximation. The solid line is the fourth cumulant, and the dashed line is the second.

sions that implies a special feature found in any of the 2D kicked rotors. Substitution gives

$$\begin{aligned} \mathcal{X}_n &\approx \int_0^1 dq \left(\ln|K \cos(2\pi q)| - \ln \frac{K}{2} \right)^n \\ &= \int_0^1 dq [\ln|\cos(2\pi q)| + \ln 2]^n, \end{aligned} \quad (24)$$

which shows that to the extent that dynamical correlations can be ignored, every cumulant is independent of the overall kicking strength. The probability density thus has a single functional form for all kicking strengths. Therefore, although the Lyapunov exponent grows logarithmically with K , the probability density of FTSEs retains the same shape and width (it just translates with ν_1 as K increases). Assuming the kicking strength is large enough that the system is strongly chaotic, any K dependence of the probability density, other than where it is centered, is due to variation of dynamical correlations and oscillatory.

Even stronger dynamical correlations and more sharply defined fluctuations show up in the higher cumulants. In Fig. 9, the fourth and second cumulants are compared.

The fourth cumulant displays much sharper features than the second. On the other hand, the features are present in the same regions of K , so the connection to stable islands is the same as for the variance. We did not carry out the corresponding time-scaling calculations as we have no reason to doubt that they reflect the stable structures for the same reasons as for the variance.

D. Fluctuations in $1/|\text{Det}(M_t - I)|$

Since higher cumulants carry information and have increased sensitivity to stable structures, a quantity that contains information from all the cumulants has the potential to be roughly optimal for its sensitivity to stable structures. Through relations such as Eq. (18), one sees that $1/|\text{Det}(M_t - I)|$ fits into this category. Furthermore, it is a

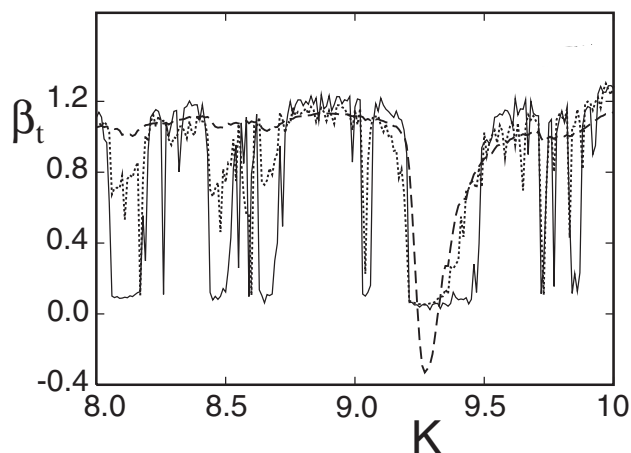


FIG. 10. The quantity β_t as a function of K at $t=100$. The averaging involved 40000 initial conditions spread uniformly across phase space. The solid line is the exact trace. The relatively smoothly behaving dashed line is what the result would be for a normal variable—i.e., $\beta_t = \nu_1 - \nu_2/2$. The dotted line derives from the $j=0$ approximation. In principle, the approximation's errors are much worse for a quantity such as β_t relative to one of the low-order cumulants, ν_n .

quantity of considerable interest in semiclassical theory, where the square root occurs as the amplitude along classical paths. We therefore define

$$\beta_t = \frac{-1}{t} \ln \left\langle \frac{1}{|\text{Det}(M_t - I)|} \right\rangle. \quad (25)$$

In a uniformly hyperbolic system, β_∞ is the Lyapunov exponent. However, if the hyperbolicity is not uniform, as is generically the case, then β_t is less than the corresponding stability exponent. In the presence of stable motion, it must tend toward vanishing. The averaging above can be done over any ensemble of phase-space trajectories over time t ; we use a uniform density over Ω . Shown in Fig. 10 is the variation of this quantity across a range of K values. Its extreme sensitivity to small islands and sticky regions of phase space is quite apparent. This may be expected as the denominator can come arbitrarily close to zero in the neighborhood of points undergoing bifurcations. We show two calculations in the figure, one of which is an “exact” evaluation based on finding the trace of M_t at large times, using a determinant method used initially for periodic orbits [33,34], and the other is by using the product ($j=0$) approximation in Eq. (7). The latter procedure is a stringent test for this approximation, and it is interesting that it picks out almost all of the “hot spots.” It is, however, much faster and easier to implement than the exact method. The smooth line shown is what one may expect from a normally distributed variable.

On comparison with α and with the variance itself, we find that the range of K where β_t deviates from that expected of a normal random variable is also reflected in these quantities. Note the consistency in all these measures with respect to structures due to stable, if small, islands in the phase space. For example, the structures around $K=8.47$ reflect

those already illustrated in Fig. 8, while those around $K=8.66$ correspond to similar islands. We again expect that higher dimensional generalizations of the approximation $j=0$ studied here will provide a method of ascertaining higher-dimensional, hard to detect, “weakly” mixed phase spaces.

V. DISCUSSION

The consideration of finite-time stability exponents has some advantages in relation to finite-time Lyapunov exponents. For one, they are more directly related to quantities that appear naturally in quantum mechanics. For another, their generalization to many-degrees-of-freedom systems tend to the Kolmogorov-Sinai entropy in the $t \rightarrow \infty$ limit. There is a local approximation just as there is for FTLEs, but the time-dependent transient may disappear exponentially fast in many cases for FTSEs and not FTLEs, depending on the averaging techniques employed. Corrections to the local approximation are also relatively simple, and the first one is sufficient to calculate improved estimates of Lyapunov exponents. We showed that this gives a leading correction to $\ln \frac{K}{2}$ of exactly $(K^2-4)^{-1}$ for the standard map. In fact, although not explicitly mentioned, we explored a wide variety of techniques, all of which failed to give this correction properly (most vanished or diverged). The corrections themselves are interesting as well. One would guess that they should lead to a Lévy process and numerically this is borne out. At least for low-order cumulants in the large kicking strength regime, the local approximation along with the first correction gives the full picture, and for many quantities the local approximation is more than sufficient.

For the standard map, the mean (first cumulant) FTSE converges rapidly to the Lyapunov exponent. This is understood to be a consequence of C_Ω tending exponentially quickly to zero with time in Eq. (17). The local approximation gives a mean FTSE that is independent of direct dynamical correlation contributions. Indirectly, in the mostly chaotic regime, the exclusion of chaotic trajectories from small regular regions (islands) would slightly alter the ergodic averaging, but never more than the relative measure of those regions. Consistent with this picture, other than small deviations, one sees very little effect of small islands on the mean FTSE.

The fluctuations behave quite the opposite. They can be investigated through the creation of a probability density for the FTSE. In the absence of small regular regions, the probability density takes on a single form, independent of system parameters (such as the kicking strength), which slowly shifts towards a Gaussian form as $t \rightarrow \infty$ of width $\pi^2/12$. Therefore, all deviations from this form must be due to dynamical correlations and, in particular, correlations introduced by the existence of small stable islands of motion. Since very strong K dependence is seen, the higher cumulants are very sensitive sensors of the presence of such non-hyperbolicity in the system. As such, they can be used as “detectors.” An important quantity which shows up in semiclassical theories, $|\text{Det}[M_t - 1]|^{-1}$, in principle, contains information carried in all of the cumulants. In fact, it may be the

most sensitive detector of dynamical correlations induced by tiny regions of nonhyperbolicity in the dynamics. All of the techniques and main results discussed have their generalizations to many-degrees-of-freedom systems. Those studies are currently underway [20].

ACKNOWLEDGMENTS

The authors gratefully acknowledge important discussions with Denis Ullmo, Alfredo Ozorio de Almeida, and Shmuel Fishman. They also gratefully acknowledge Roland Ketzmerick for finding the kicking strength of the double saddle node bifurcation, and S.T. gratefully acknowledges support from U.S. National Science Foundation Grant No. PHY-0555301.

APPENDIX A

The relation is

$$\text{Tr}[M_t(q_0, p_0)] = \sum_{j=0}^{\lfloor t/2 \rfloor} (-1)^j \sum_{\substack{\text{odd} \\ \text{arrng}}} \prod_{\substack{t-2j \\ \text{factors} \\ k}} [2 - V''(q_{\{i,k\}})], \quad (\text{A1})$$

where $\lfloor t/2 \rfloor$ is the integer part of $t/2$ and the odd arrangements of the product of $t-2j$ factors is specified just ahead. Also note that if t is even, the final term (the one for which $j=t/2$) is $(-1)^{t/2} \times 2$.

There are two key properties required for the above identity. First, there must exist at least one column or row in the set of $\{M(q_i)\}$ both of whose elements are the same constants for all members of the set. Second, the determinants of the set of $\{M(q_i)\}$ must all be equal to the same value (if this value is not equal to unity, then the terms in the equation above must be multiplied by its j th power).

It turns out there is a fairly simple rule for which products can contribute to a particular “ j term.” Imagine the t integers $\{i \in [0, t-1]\}$ uniformly spaced on a ring. Those are the “locations” that each factor in a product can occupy, so to speak, determined by its own subscript. For a given time t with $t-2j$ factors in the product, each arrangement that has exclusively odd-unit spacings between occupied locations contributes once to that j term. All cyclically connected arrangements are automatically included in this construction, and thus the cyclic invariance of the trace is easy to see. The number of such odd-spacing arrangements \mathcal{N}_A turns out to be

$$\mathcal{N}_A = \frac{t}{t-j} \binom{t-j}{j}, \quad (\text{A2})$$

which is related to the summation and recursion relation

$$\begin{aligned} S(t, j) &= \frac{1}{j!} \frac{d^j}{dx^j} [(1 + \sqrt{x})^t + (1 - \sqrt{x})^t]_{x=1} \\ &= 2 \sum_{m=j}^{\lfloor t/2 \rfloor} \binom{t}{2m} \binom{m}{j} = 2^{t-2j} \frac{t}{t-j} \binom{t-j}{j}. \end{aligned} \quad (\text{A3})$$

The combinatorials are related to an expansion of the functional form of eigenvalues raised to various powers of a two-

by-two matrix. The $j=0$ term is simply the product of all factors

$$\text{Tr}[M_t(q_0, p_0)]_{j=0} = \prod_{i=0}^{t-1} [2 - V''(q_i)]. \quad (\text{A4})$$

One could also label this term $\{1^t\}$, indicating that there are t unit spacings. Similarly, the $j=1$ term is always the cyclic sum $\{1^{t-3}, 3\}$ of which there are t terms. Thus,

$$\begin{aligned} \text{Tr}[M_t(q_0, p_0)]_{j=0+1} &= \prod_{i=0}^{t-1} [2 - V''(q_i)] \left(1 - \sum_i^{\text{cyclic}} \frac{1}{[2 - V''(q_i)][2 - V''(q_{i+1})]} \right), \end{aligned} \quad (\text{A5})$$

where the last term has indices $(t-1, 0)$. Pulling the product of all factors out front emphasizes that if the $\{V''(q_i)\}$ are generally much larger than 2, then for times not too long the $j>0$ terms can be thought of as corrections, each successive one roughly proportional to $t \langle (V'')^2 \rangle^{-1}$ weaker than the previous term. In some sense, the first nontrivial j term comes for $t=6$ and $j=2$. One expects nine double products of factors. The allowed odd-spacing arrangements are $\{1, 5\}$ and $\{3, 3\}$. There are six terms related to the cyclic permutations of the $i(i+1)$ product ($\{1, 5\}$) and only three terms for the $i(i+3)$ product ($\{3, 3\}$) since it repeats itself after half a cycle, and thus 9, the correct count of terms, is consistent with Eq. (A2). The above expression is the expansion of the determinant given by Bountis and Helleman [33] nearly 30 years ago. Greene developed its small- K expansion in his study of the behavior of KAM surfaces [34].

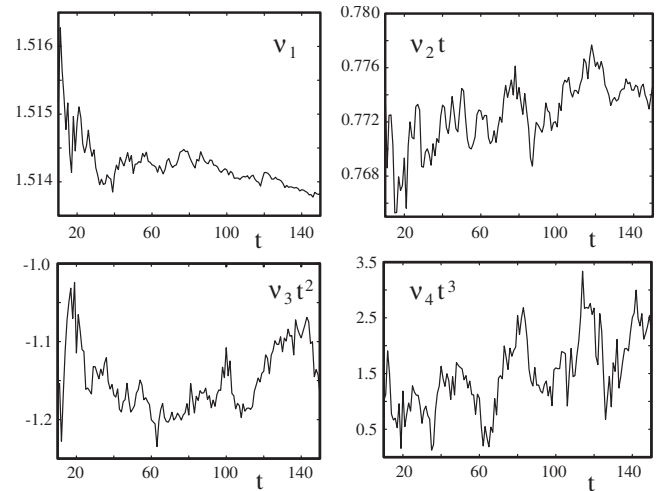


FIG. 11. The first four cumulants as a function of time. The cumulants are multiplied by the time factors needed to make them independent of time according to the expressions leaving out dynamical correlations. The kicking strength is 8.9633781407, which gives the prediction that the Lyapunov exponent (first cumulant) is equal to 1.513.

APPENDIX B

It is more convenient to focus on the cumulants than the central moments as it simplifies the time dependence. There is also the advantage of interpretation of the probability density. For a Gaussian density, only the first two cumulants are nonzero. For other densities, the higher cumulants describe shape deviations. There is a third advantage, which comes into play when considering the relationship with quantum mechanics, but we do not elaborate here. If the dynamical correlations vanish or are small enough to be ignored, then the expression for the cumulants can be simplified. With these quantities, the cumulants have the same polynomial form P_n as with the central moments and a very simple dependence on t .

The result is

$$\nu_n(t) = t^{1-n} P_n. \quad (\text{B1})$$

For example,

$$\nu_3(t) = \frac{1}{t^2} \mathcal{X}_3,$$

$$\nu_4(t) = \frac{1}{t^3} (\mathcal{X}_4 - 3\mathcal{X}_2^2). \quad (\text{B2})$$

An amusing, known consequence of the time dependence in Eq. (B1) is that there is a sense in which the distribution collapses to a δ -function density as $t \rightarrow \infty$ as expected (every trajectory has the same Lyapunov exponent), and the time dependence of the reduced cumulants goes as

$$\tilde{\nu}_n(t) = \frac{\nu_n(t)}{\nu_2^{n/2}(t)} \propto t^{1-n/2}, \quad (\text{B3})$$

which for $n \geq 3 \rightarrow 0$ as $t \rightarrow \infty$. In other words, the density slowly approaches a Gaussian form. Nevertheless, the δ -function limit is approached slowly enough that the width of the probability density for $|\text{Tr}(M_t)|$ grows without bound as t increases, and it is not well approximated by a lognormal density. An example of the time dependence of the first four cumulants for a kicked rotor can be seen in Fig. 11. It illustrates that the time dependence is to within fluctuations as predicted for K values at which dynamical correlations are not observed.

-
- [1] A. J. Lichtenberg and M. A. Lieberman, *Regular and Chaotic Dynamics* (Springer, New York, 1992).
- [2] E. Ott, *Chaos in Dynamical Systems* (Cambridge University Press, New York, 1997).
- [3] H. Fujisaka, *Prog. Theor. Phys.* **70**, 1264 (1983).
- [4] J. Theiler and L. A. Smith, *Phys. Rev. E* **51**, 3738 (1995).
- [5] A. Prasad and R. Ramaswamy, *Phys. Rev. E* **60**, 2761 (1999).
- [6] C. Anteneodo, *Phys. Rev. E* **69**, 016207 (2004).
- [7] M. A. Sepúlveda, R. Badii, and E. Pollak, *Phys. Rev. Lett.* **63**, 1226 (1989).
- [8] C. Amitrano and R. S. Berry, *Phys. Rev. Lett.* **68**, 729 (1992).
- [9] C. Amitrano and R. S. Berry, *Phys. Rev. E* **47**, 3158 (1993).
- [10] D. Beigie, A. Leonard, and S. Wiggins, *Phys. Rev. Lett.* **70**, 275 (1993).
- [11] G. Lapeyre, *Chaos* **12**, 688 (2002).
- [12] P. E. Arratia and J. P. Gollub, *J. Stat. Phys.* **121**, 805 (2005).
- [13] A. Crisanti, G. Paladin, and A. Vulpiani, *Products of Random Matrices in Statistical Physics* (Springer-Verlag, Berlin, 1993).
- [14] A. B. Rechester and R. B. White, *Phys. Rev. Lett.* **44**, 1586 (1980).
- [15] I. Goldhirsch, P.-L. Sulem, and S. A. Orszag, *Physica D* **27**, 311 (1987).
- [16] M. C. Gutzwiller, *Chaos in Classical and Quantum Mechanics* (Springer-Verlag, New York, 1990).
- [17] P. G. Silvestrov, J. Tworzydło, and C. W. J. Beenakker, *Phys. Rev. E* **67**, 025204(R) (2003).
- [18] B. V. Chirikov, *Phys. Rep.* **52**, 263 (1979).
- [19] J. M. Greene and J.-S. Kim, *Physica D* **24**, 213 (1987).
- [20] S. Tomsovic and A. Lakshminarayan (unpublished).
- [21] P. Grassberger, R. Badii, and A. Politi, *J. Stat. Phys.* **51**, 135 (1988).
- [22] H. D. I. Abarbanel, R. Brown, and M. B. Kennel, *J. Nonlinear Sci.* **1**, 175 (1991).
- [23] B. Eckhardt and D. Yao, *Physica D* **65**, 100 (1993).
- [24] R. S. MacKay, J. D. Meiss, and I. C. Percival, *Physica D* **27**, 1 (1987).
- [25] H. Schomerus and M. Titov, *Phys. Rev. E* **66**, 066207 (2002).
- [26] M. W. Beims, C. Manchein, and J.-M. Rost (unpublished).
- [27] V. Constantoudis and N. Theodorakopoulos, *Phys. Rev. E* **56**, 5189 (1997).
- [28] P. Grassberger and H. Kantz, *Phys. Lett.* **113A**, 167 (1985).
- [29] T. Horita, H. Hata, R. Ishizaki, and H. Mori, *Prog. Theor. Phys.* **83**, 1065 (1990).
- [30] G. M. Zaslavsky, *Phys. Rep.* **371**, 461 (2002).
- [31] R. Ishizaki, T. Horita, T. Kobayashi, and H. Mori, *Prog. Theor. Phys.* **85**, 1013 (1991).
- [32] P. Duarte, *Ann. Inst. Henri Poincaré Anal. Non Linéaire* **11**, 359 (1994).
- [33] T. Bountis and R. H. G. Helleman, *J. Math. Phys.* **22**, 1867 (1981).
- [34] J. M. Greene, *J. Math. Phys.* **20**, 1183 (1979).